Validation of Clausius–Mossotti Function in Wideband Single-Cell Dielectrophoresis

Xiaotian Du, *Student Member, IEEE*, Xiao Ma, *Student Member, IEEE*, Hang Li, *Member, IEEE*, Lei Li, *Student Member, IEEE*, Xuanhong Cheng, and James C. M. Hwang, *Life Fellow, IEEE*

***Abstract*—For the first time, both lower and upper crossover frequencies of the real part of the Clausius–Mossotti function were calculated by using cell parameters measured on the same ultrawideband setup as that for single-cell dielectrophoresis. The calculation suggests that the lower crossover frequency can be from 0 to 127 kHz and that the upper crossover frequency can be from 45 to 108 MHz, in the unlikely case when uncertainties in the cell parameters all add up. The calculated lower crossover frequency was found to be in general agreement with the measured values of 28 ± 4 kHz. However, the calculated upper crossover frequency was significantly different from the measured values of 326 ± 35 MHz. The difference can be attributed to the field being highly nonuniform in single-cell dielectrophoresis, especially at higher frequencies. Additionally, with closely spaced electrodes in single-cell dielectrophoresis, adhesive force may have to be considered, even for a relatively nonadherent Jurkat cell. In any case, the difference between the calculated and measured crossover frequency suggests that the classical Clausius–Mossotti function, originally derived from the Maxwell–Wagner mixture model of a cell suspension, may not apply to single-cell dielectrophoresis in a straightforward manner, especially at high frequencies.**

***Index Terms*—Biological cells, biosensors, cellular biophysics, dielectrophoresis, microwave measurements, ultra-wideband technology.**

I. Introduction

Dielectrophoresis (DEP) was first observed on small plastic particles that were neutral, spherical, homogenous, and suspended in a conductive solution [1]. When the particles were polarized by an applied electric field, they would be forced to move if the field was not uniform. Because the particles would

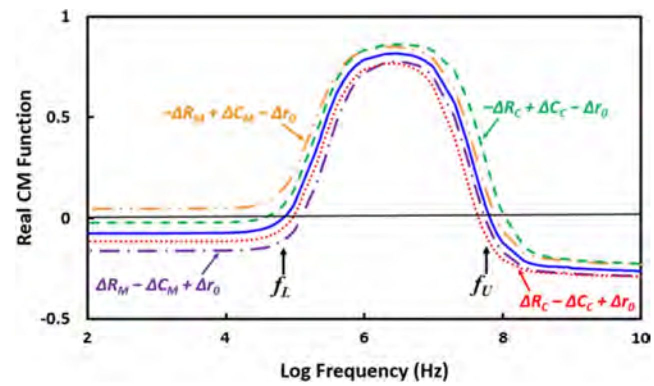

Fig. 1. Calculated frequency dependence of the real part of the Clausius-Mossotti function for a Jurkat cell suspended in sucrose solution (solid curve). The combined effects of deviations in membrane resistance ΔR_M, membrane capacitance ΔC_M, cytoplasm resistance ΔR_C, cytoplasm capacitance ΔC_C, and cell radius Δr_0 are also included (dotted and dashed curves).

move along the field gradient instead of the field direction as charged particles would, alternating-current (AC) DEP could be used to move the particles one way while avoiding electrode polarization. In this case, the time-averaged moving force F is related to the field gradient ∇E (root-mean-square-averaged across the particle) by the real part of the Clausius-Mossotti function $f_{CM}(\omega)$, where $\omega = 2\pi f$ is the angular frequency of the applied AC DEP signal. Thus

$$F = 2\pi \varepsilon_S r_0^3 \mathrm{Re}\left[f_{CM}(\omega)\right] \nabla |E|^2 \quad (1)$$

and

$$f_{CM}(\omega) = \left(\varepsilon_P^* - \varepsilon_S^*\right) / \left(\varepsilon_P^* + 2\varepsilon_S^*\right) \quad (2)$$

where r_0 is the particle radius, $\varepsilon^*_P = \varepsilon_P - j\sigma_P/\omega$, and $\varepsilon^*_S = \varepsilon_S - j\sigma_S/\omega$ are the complex permittivities of the particle and solution, respectively. Assuming $f \leq$ 100 MHz so that ε_S is constant, $f_{CM}(\omega)$ captures all the frequency dependence of F through the dispersion of ε^*_P and ε^*_S.

As illustrated in Fig. 1, depending on f, Re[$f_{CM}(\omega)$] can be positive or negative, so that the particle can move toward the field maximum or minimum, which is referred to as positive DEP (pDEP) or negative DEP (nDEP). For a homogeneous particle, $f_{CM}(\omega)$ is independent of the particle size or shape. For a heterogeneous biological cell, ε^*_P can have subtle dependence on the cell size/shape, but $f_{CM}(\omega)$ is much less sensitive to the cell size/shape than F is. For this reason, the DEP crossover frequencies (from nDEP to pDEP or vice versa) instead of the

Manuscript received August 20, 2018; revised November 28, 2018; accepted January 9, 2019. Date of publication January 18, 2019; date of current version May 10, 2019. This work was supported in part by the U.S. Department of Defense, Defense Treat Reduction Agency under Grant HDTRA1-12-1-0007, in part by the Army Research Office under Grant W911NF-14-1-0665, in part by the Air Force Office of Scientific Research under Grant FA9550-16-1-0475, and in part by the National Science Foundation under Grant ECCS-1809623. This paper was presented in part at the IEEE MTT-S International Microwave Biomedical Conference, Philadelphia, PA, USA, June 2018. *(Corresponding author: Xiaotian Du.)*

X. Du, X. Ma, L. Li, and J. C. M. Hwang are with the Department of Electrical and Computer Engineering, Lehigh University, Bethlehem, PA 18015 USA (e-mail: xid415@lehigh.edu; xim214@lehigh.edu; lel216@lehigh.edu; jh00@lehigh.edu).

H. Li was with the Department of Bioengineering, Lehigh University, Bethlehem, PA 18015 USA. He is now with the School of Medicine, University of California, San Francisco, CA 94143 USA (e-mail: Hang.Li@ucsf.edu).

X. Cheng is with the Department of Bioengineering and the Department of Materials Science and Engineering, Lehigh University, Bethlehem, PA 18015 USA (e-mail: xuc207@lehigh.edu).

Digital Object Identifier 10.1109/JERM.2019.2894100

DEP force are often exploited in sorting biological cells. Furthermore, the lower crossover frequency f_L is more popular than the upper crossover frequency f_U, because f_L is better suited to the bandwidth of most DEP setups. However, f_U promises even weaker dependence on the cell size/shape and higher sensitivity to the cytoplasm property of a cell [2].

DEP has been widely used as a fast and label-free means to manipulate or characterize a population of biological cells suspended in a solution [2]. In particular, DEP of different frequencies was used to separate cells whose membrane conductivity was enhanced by electroporation [3]. The effect of membrane conductivity and nonspherical shape was explored theoretically [4]. The lower crossover frequency f_L was used to determine the cytoplasm conductance, although at low frequencies the membrane contribution could not be ruled out [5].

Recently, DEP displacement at 10 MHz of a single cell was used to measure the change in cytoplasm conductivity after electroporation [6]. Dual-frequency DEP of a single cell was used to determine the membrane capacitance at 100 kHz and the cytoplasm conductivity at 6 MHz [7]. Multi-frequency DEP was used to determine the changes in membrane capacitance and cytoplasm conductance of a single cell after thermal stress [8]. With multiple frequencies at 300 kHz, 600 kHz, and 6 MHz, the effects of membrane conductance, membrane capacitance, and cytoplasm conductance could be better differentiated. However, the most prominent feature of the measured data was the shift of f_L resulting from changes in both membrane conductance and membrane capacitance.

By contrast, with a bandwidth of 100 kHz–300 MHz, the upper crossover frequency f_U around 100 MHz was used to separate single cells of different cell lines [9] or of the same cell line but cultured under different conditions [10]. It was argued that f_U was more effective in separating cells of different cytoplasm properties [11].

For either f_L or f_U, it is not obvious that (2), originally derived from the Maxwell–Wagner mixture model of a cell suspension [2], applies to single-cell DEP. In particular, single-cell DEP typically uses small and closely spaced electrodes, so that the electric field can be greatly disturbed by the presence of a cell and the resulted field distribution can be highly nonuniform across the cell [12]. Most recently, with a 9 kHz–9 GHz ultra-wideband (UWB) setup, we validated f_L for a Jurkat T-lymphocyte human cell in an isotonic sucrose solution [13]. This paper expands on [13] mainly by deriving $f_{CM}(\omega)$ from lumped cell resistances and capacitances instead of cell dielectric constants and conductivities, and by quantifying the effects of cell resistances and capacitances on $f_{CM}(\omega)$. The derived f_L and f_U were both compared with experimental data, whereas [13] only validated f_L.

II. Theory

Previously, we used literature values of ε^*_P to evaluate (2) and neglected the contribution of the membrane resistance R_M [13]. We now attempt to improve the accuracy by including R_M, as well as by using our own experimentally measured values based on the same cell line and UWB setup.

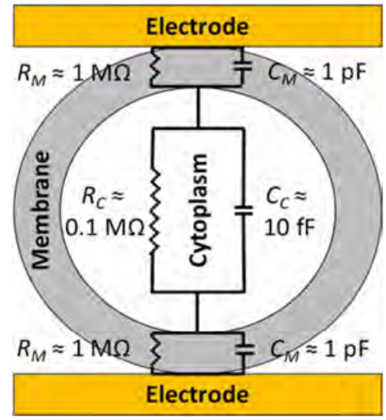

Fig. 2. A single-shell model of a cell overlaid by its equivalent circuit.

For a Jurkat cell in isotonic sucrose solution, we have extracted through UWB impedance spectroscopy the lumped equivalent circuit parameters of the cell as shown in Fig. 2 [14]. Specifically, $R_M = 1.5 \pm 0.3\,\text{M}\Omega$, $C_M = 1.5 \pm 0.3\,\text{pF}$, $R_C = 0.4 \pm 0.1\,\text{M}\Omega$, and $C_C = 6.4 \pm 0.1\,\text{fF}$, where C_M is the membrane capacitance, R_C is the cytoplasm resistance, and C_C is the cytoplasm capacitance. These lumped parameters can be converted to distributed membrane and cytoplasm parameters $\varepsilon^*_M = \varepsilon_M - j\sigma_M/\omega$ and $\varepsilon^*_C = \varepsilon_C - j\sigma_C/\omega$ as shown in the following.

To relate R_C and C_C with ε_C and σ_C, we first assume a uniform field E inside the cell [15]

$$E = qn_0/3\varepsilon_C \tag{3}$$

where q is the electron charge, and n_0 is an area density constant. The induced charge distribution ρ on the cell membrane is dipole-like as

$$\rho(\theta) = qn_0 \cos\theta \tag{4}$$

where θ is the angle with respect to the normal of the electrodes. The potential ϕ inside the cell is

$$\phi(r, \theta) = n_0 r \cos\theta / 3\varepsilon_C \tag{5}$$

where $r \le r_0$ is the distance from the center of the cell. The potential is relative to the horizontal plane of symmetry that bisect the cell because $\phi(0, \pi/2) = 0$. Thus, the total charge Q over one half of the cell membrane can be calculated by integrating the membrane charge density over a hemispherical surface

$$Q = \int_0^{\pi/2} (n_0 \cos\theta)(2\pi r_0 \sin\theta) r_0 d\theta = \pi q n_0 r_0^2. \tag{6}$$

The voltage difference V between the north and south poles of the cell is

$$V = q[\phi(r_0, 0) - \phi(r_0, \pi)] = 2qn_0 r_0/3\varepsilon_C. \tag{7}$$

Based on the homogeneous-cytoplasm and uniform-field assumptions, the current density across the cell is also uniform as $qn_0\sigma_C/3\varepsilon_C$. Therefore, it can be multiplied by the cross-section

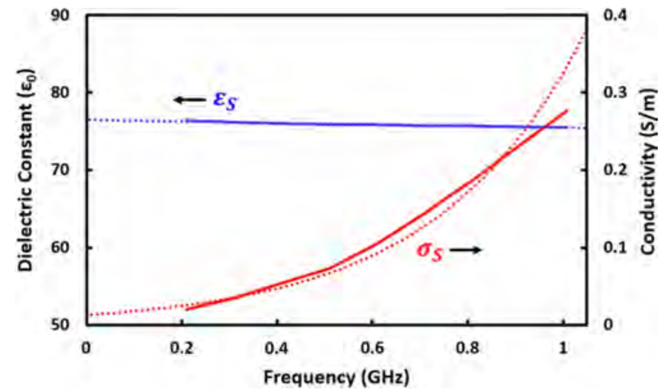

Fig. 3. Measured (solid) vs. fitted (dotted) dielectric constant ε_S and conductivity σ_S of the sucrose solution.

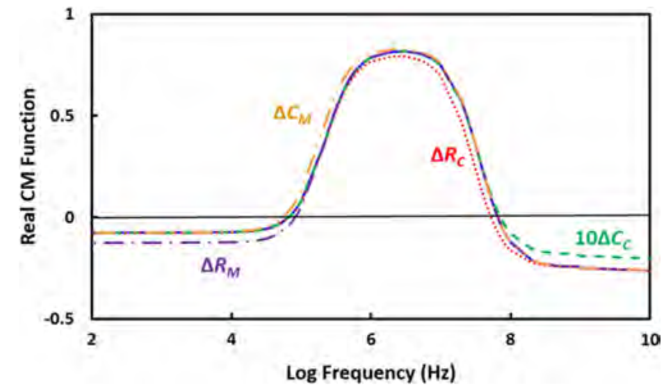

Fig. 4. Calculated effects on the real part of the Clausius-Mossotti function by adding standard deviations to the experimentally extracted values of R_M, C_M, R_C, and C_C, with the effect of ΔC_C exagerated ten times to make it visible.

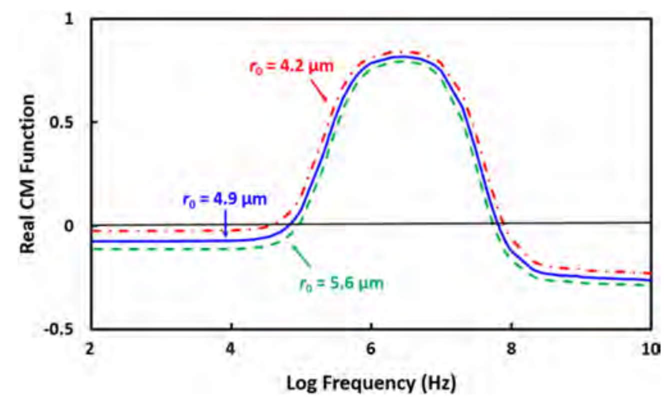

Fig. 5. Calculated effects on the real part of the Clausius-Mossotti function by varying the cell radius r_0 from 4.2, 4.9, to 5.6 µm.

area of the cell to obtain the total current I across the cell

$$I = \pi q n_0 r_0^2 \sigma_C / 3\varepsilon_C. \tag{8}$$

Thus

$$R_C = V/I = 2/\pi r_0 \sigma_C \tag{9}$$

and

$$C_C = Q/V = 3\pi r_0 \varepsilon_C / 2. \tag{10}$$

Therefore, ε_M, σ_M, ε_C, and σ_C can be expressed in terms of C_M, R_M, C_C, and R_C as in the following:

$$\varepsilon_M = tC_M/4\pi r_0^2 = (2.8 \pm 0.5)\,\varepsilon_0 \tag{11}$$

$$\sigma_M = t/4\pi r_0^2 R_M = 11 \pm 2.8\ \mu\text{S/m} \tag{12}$$

$$\varepsilon_C = 2C_C/3\pi r_0 = (31.3 \pm 0.5)\,\varepsilon_0 \tag{13}$$

and

$$\sigma_C = 2/\pi r_0 R_C = 0.3 \pm 0.1\ \text{S/m} \tag{14}$$

where ε_0 is the vacuum permittivity, $t \approx 5$ nm is the assumed membrane thickness [16], and $r_0 = 4.9 \pm 0.7$ µm is the measured cell radius by using a Beckman Z2 Coulter Counter.

The permittivity of the whole cell is [17]

$$\varepsilon_P^* = \varepsilon_M^* \frac{2(1-\alpha)\,\varepsilon_M^* + (1+2\alpha)\,\varepsilon_C^*}{(2+\alpha)\,\varepsilon_M^* + (1-\alpha)\,\varepsilon_C^*} \tag{15}$$

where the volume ratio $\alpha = r_0^3 / (r_0 + t)^3$. With $\delta = t/r_0 << 1$, $\alpha \approx 1 - 3\delta$, and

$$\varepsilon_P^* \approx \varepsilon_M^* \frac{2\delta\varepsilon_M^* + (1-2\delta)\,\varepsilon_C^*}{(1-\delta)\,\varepsilon_M^* + \delta\varepsilon_C^*}. \tag{16}$$

Substituting (16) into (2), we can evaluate $\mathrm{Re}[f_{CM}(\omega)]$ provided ε^*_S is known. For the present sucrose solution, we have used an Agilent 85070 dielectric probe to determine that $\varepsilon_S = (76.4 - 10^{-9} f)\,\varepsilon_0$ and $\sigma_S = 0.013 \exp(3 \times 10^{-9} f)$ S/m as shown in Fig. 3.

Fig. 1 shows the calculated frequency dependence of $\mathrm{Re}[f_{CM}(\omega)]$ for a Jurkat cell suspended in sucrose solution using experimentally measured R_M, C_M, R_C, and C_C. It can be seen that $f_L = 65$ kHz and $f_U = 66$ MHz, respectively. These frequencies are significantly different from 50 kHz and 800 MHz obtained by using parameter values from the literature [13], especially for f_U due to the differences in ε_C and σ_C.

Fig. 4 shows the effects of adding standard deviations ΔR_M, ΔC_M, ΔR_C, and $10\,\Delta C_C$ to $\mathrm{Re}[f_{CM}(\omega)]$. Due to the UWB bandwidth used in the measurement [14], the precision $\Delta C_C/C_C$ is much better than $\Delta R_M/R_M$, $\Delta C_M/C_M$, or $\Delta R_C/R_C$, so the effect of ΔC_C is artificially exaggerated ten times to make it visible. It can be seen that f_L is mainly sensitive to membrane properties R_M and C_M. When R_M is increased to $R_M + \Delta R_M$, f_L shifts from 65 kHz to 81 kHz. When C_M is increased to $C_M + \Delta C_M$, f_L shifts from 65 kHz to 55 kHz. On the other hand, f_U is mainly sensitive to cytoplasm properties R_C and C_C. With $R_C = R_C + \Delta R_C$, f_U shifts from 66 MHz to 53 MHz. With $C_C = C_C + 10\,\Delta C_C$, f_U shifts from 66 MHz to 70 MHz. Note that [7] specifies that f_L is sensitive to C_M only, whereas [11] did not specify whether f_U is sensitive to R_C or C_C. Fig. 4 shows also that the magnitude of the DEP force is mainly sensitive to R_M for $f < f_L$, R_C for $f_L < f < f_U$, and C_C for $f > f_U$. Note [8] also specifies that the DEP force is mainly sensitive to R_M for $f < f_L$, and R_C for $f_L < f < f_U$.

Even if a cell line is cloned with uniform R_M, C_M, R_C, and C_C, its natural size distribution can cause ε^*_P to vary according to (11)–(14). Fig. 5 shows the effect of $\pm\,\Delta r_0$, which shifts f_L and f_U to 35–90 kHz and 56–80 MHz, respectively.

The above calculations use all experimentally measured parameter values except the membrane thickness t, which may deviate from the assumed value of 5 nm. However, $f_{CM}(\omega)$ is not very sensitive to Δt, because it affects only ε^*_M and the effect on ε^*_M is largely cancelled out on ε^*_P due to small δ and the fact $\varepsilon^*_M << \varepsilon^*_C$. Specifically, from (11) and (12), $\varepsilon^*_M(1 + \Delta t/t) = (1 + \Delta t/t)\,\varepsilon^*_M(t)$. From (16)

$$\begin{aligned}
&\varepsilon^*_P(t + \Delta t)\\
&\quad\approx (1 + \Delta t/t)\,\varepsilon^*_M(t)\frac{2\delta\,(1 + \Delta tt)\,\varepsilon^*_M(t) + (1 - 2\delta)\,\varepsilon^*_C}{(1-\delta)\,(1 + \Delta t/t)\,\varepsilon^*_M(t) + \delta\varepsilon^*_C}\\
&\quad\approx \varepsilon^*_M(t)\,\frac{2\delta\varepsilon^*_M(t) + (1 - 2\delta)\,\varepsilon^*_C}{\varepsilon^*_M(t) + \delta\varepsilon^*_C}\\
&\quad\approx \varepsilon^*_P(t).
\end{aligned} \tag{17}$$

In summary, the above calculations show that f_L is mainly sensitive to cell size r_0 and membrane properties R_M and C_M, whereas f_U is mainly sensitive to cell size r_0 and cytoplasm properties R_C and C_C. When the effects of ΔR_M, ΔC_M, and Δr_0 are added up, f_L can vary from 0 to 127 kHz, suggesting that in the extreme case f_L may disappear altogether. On the other hand, when the effects of ΔR_C, ΔC_C, and Δr_0 are added up, f_U can vary from 45 MHz to 108 MHz. These estimated ranges of f_L and f_U have been included in Fig. 1. Note that in reality the extremes of ΔR_M, ΔC_M, ΔR_C, ΔC_C, and Δr_0 rarely occur simultaneously.

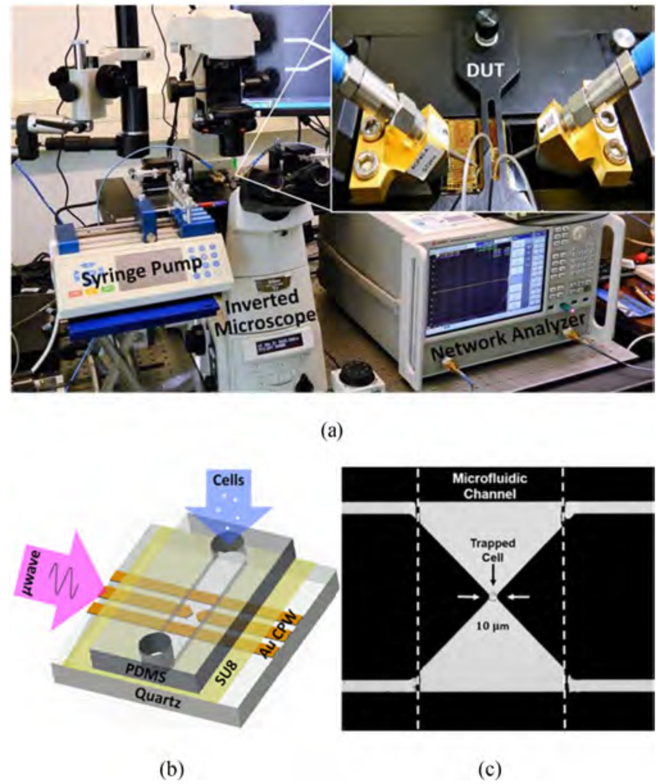

Fig. 6. (a) Photograph of the experimental set up and (b) schematic and (c) micrograph of the device under test. In (c), a Jurkat cell is trapped between two tapered sections of the center electrode of a coplanar waveguide, which are 10-µm apart. Dashed lines delineate the microfluidic channel.

III. Experimental Setup and Procedure

Fig. 6(a) shows that the present UWB DEP setup is similar to that of [13] except in the detailed electrode construction. The setup comprises a homemade microwave probe station on top of a Nikon Eclipse TE2000 inverted fluorescence microscope, which is equipped with a Hamamatsu Flash 4.0 V2 100-frame/s three-color video camera. A Keysight E5080A 9 kHz-9 GHz vector network analyzer (VNA) is used to apply the DEP signal to the device under test (DUT) via a pair of Cascade Microtech ACP40 GSG probes with a pitch of 200 µm. A Fusion 400 syringe pump is used to inject the cells into the microfluidic channel of the DUT.

Fig. 6(b) shows schematically that the DUT comprises four main layers: a PDMS cover, an SU8 wall, a gold coplanar waveguide (CPW), and a quartz substrate. The width, length, and thickness of the PDMS cover are 5 mm, 8 mm and 4 mm, respectively, after curing from a mixture of 10:1 base-to-agent ratio. The 20-µm-tall SU8 walls are precisely defined by photolithography to be 2.4-mm wide and 200-µm apart. Thus, the microfluidic channel is 20-µm tall and 200-µm wide. The microfluidic channel intersects the CPW at a right angle. The CPW is 1-cm long with its center electrode being mostly 200-µm wide except under the microfluidic channel, where it is tapered down to 10 µm with a 10-µm gap in the middle for DEP trapping of a cell as shown in Fig. 6(c). Each ground electrode of the CPW is 200-µm wide. Outside the microfluidic channel, the gap between the center electrode and the ground electrodes of the CPW is 16-µm wide. The CPW is designed with a 50-Ω characteristic impedance across a UWB of 9 kHz-9 GHz before the tapers [14]. The CPW is 0.5-µm thick, whereas the quartz substrate is 500-µm thick. A 15-nm-thick Ti layer is inserted between gold and quartz to enhance adhesion. The main difference of the electrode construction from that of [13] is that the present electrode is 0.5-µm thick instead of 2-µm thick, which allows the electrode to be tapered more sharply.

For proof of concept, Jurkat cells were chosen for their relatively simple structure, large diameter, and nonadherent nature. Similar to [13], cells were cultured in RPMI 1640 supplemented with 10% fetal bovine serum, 100 unit/mℓ penicillin, and 100 µg/mℓ streptomycin in a 37 °C, 5% CO_2 incubator. Cells were twice washed before resuspension in an isotonic solution with 8.5% sucrose and 0.3% dextrose to a concentration of 3×10^6 cell/mℓ. The resuspended cells were injected into the microfluidic channel at a rate of 0.1 µℓ/min. Cell viability was tested in a separate experiment with trypan blue staining, which showed more than half of cells survived the sucrose solution after 10 h [18].

Jurkat cells were trapped singularly by a 0-dBm 5-MHz pDEP signal generated by the VNA. Proper trapping was verified through the microscope as shown in Fig. 6(c), before the flow was reduced to a creep to avoid dislodging the cell without the pDEP signal. To avoid the complication of fluid dynamics, crossover frequencies were measured through detrapping instead of trapping experiments. To measure f_L, the VNA was programmed to generate a 3-dBm nDEP signal with its

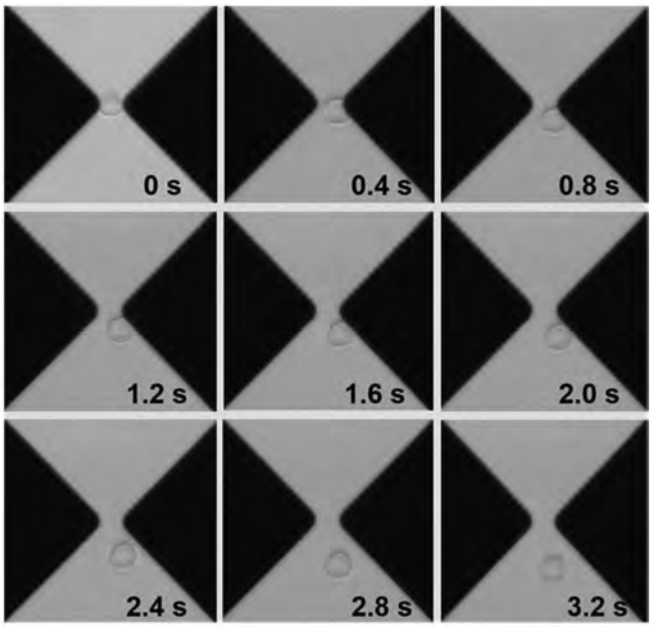

Fig. 7. Sequential micrographs of the detrapping of a Jurkat cell under an nDEP signal of 6 dBm and 400 MHz.

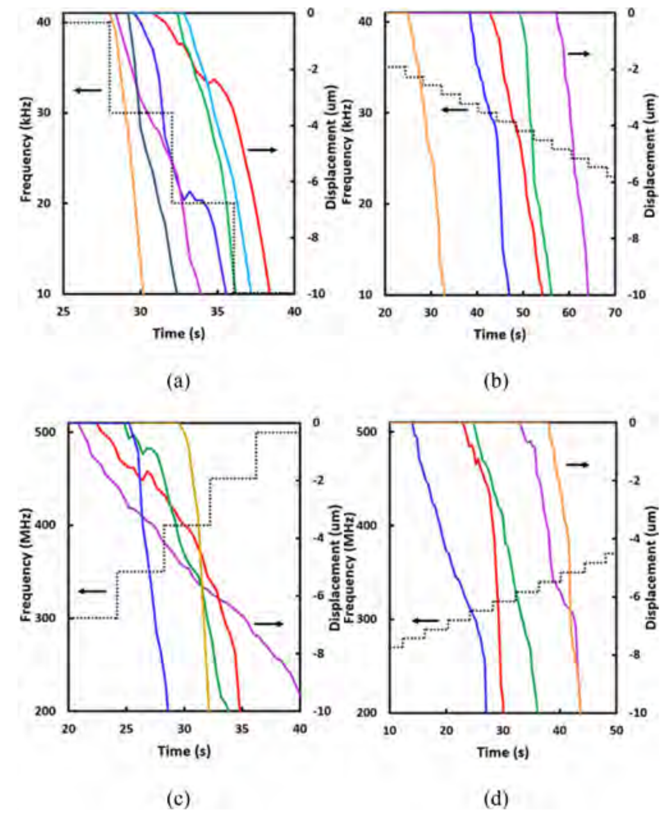

Fig. 8. DEP signal waveform and cell displacement trajectory for (a), (b) low-frequency and (c), (d) high-frequency detrapping of a Jurkat cell. The experiment was repeated seven times in (a) and five times in (b)–(d). Each time a different cell was used.

frequency stepping down from 100 kHz to 10 kHz by 5 kHz every 4 s in the first set of experiments to determine the range of f_L, and from 40 kHz to 20 kHz by 1 kHz every 4 s in the second set of experiments to determine the precise value of f_L. To measure f_U, the VNA was programmed to generate a 6 dBm nDEP signal with its frequency stepping up from 50 MHz to 2000 MHz by 50 MHz every 4 s first, and from 250 MHz to 350 MHz by 10 MHz every 4 s later. (Higher power was needed for nDEP than for pDEP especially for f_U as implied by Fig. 1.) Meanwhile, micrographs were recorded every 0.4 s and post-processed by the Nikon AR Elements software to quantify the cell displacement at any given moment. Fig. 7 illustrates the recorded displacement trajectory of a detrapped cell.

IV. Results and Discussion

Fig. 8 shows the DEP signal waveforms and the cell displacement trajectory for detrapping experiments at both kilohertz and megahertz frequencies. The experiment was repeated twelve times on twelve different cells at kilohertz frequencies, and ten times on ten different cells at megahertz frequencies. For each experiment, it is the onset of the displacement that matters, the exact trajectory after detrapping is not of interest. Nevertheless, the trajectory shows that there is sufficient dwell time at each frequency step for a cell to be detrapped if the frequency is sufficiently low or high. Once detrapped, the cell is completely detrapped as indicated by greater than 10 μm displacement. Based on where each trajectory intercepts the horizonal axis of zero displacement, f_L or f_U can be read from the DEP signal waveform for the frequency at that particular moment. There is no significant difference between the first [Fig. 8(a) and Fig. 8(c)] and second [see Fig. 8(b) and (d)] sets of experiment, even though the second set of experiment was performed months later on a new batch of freshly cultured cells and involved narrower frequency range and step. Therefore, they were combined in calculating the average and standard deviation of f_L or f_U.

From Fig. 8, it can be concluded that $f_L = 28 \pm 4\,\text{kHz}$ and $f_U = 326 \pm 35\,\text{MHz}$. Thus, although the measured f_L is within its theoretical range, the difference between the measured and calculated f_U is too large to be explained by either the measurement uncertainty, the theoretical parameter uncertainty, or in combination. This difference can be attributed to the field being highly nonuniform, especially at higher frequencies, so that (11)–(14) need to be modified according to the actual field distribution, which can only be done through finite-element simulation [12]. The difference between the presently measured f_L and that of [13] can be attributed to the difference in the detailed electrode design.

As shown in Fig. 1, the calculated f_U increases with increasing C_C but decreases with increasing R_C. Since the calculated f_U is lower than the measured f_U, it is possible that (13) underestimates ε_c. If ε_c is increased from 31 to 77 ε_0 (close to the dielectric constant of water at room temperature), f_U will increase to 369 MHz, which will be in the range of the measured f_U.

Presently, pDEP and nDEP are used to quickly trap and detrap a cell so that rapidly successive measurements can be performed to extract the small cell signal from the background signal, amounting to an interferometer in time domain instead of spatial domain [19]. As shown in Fig. 8, trapping and detrapping usually occur in a few seconds so that the entire sequence of trapping, characterization, and detrapping can be conveniently completed on the order of 1 min [20]. Under such conditions, it is unlikely that DEP can alter the state of the cell, especially in view of the fact that much higher power of at least 9 dBm is required to trigger electroporation or otherwise affect cell vitality [21]. The absence of heating by DEP is confirmed by a temperature-sensitive dye under an even stronger signal of approximately 15 dBm [12]. Lastly, DEP does not appear to significantly alter the shape and size of the cell as shown in Fig. 7.

V. Conclusion

In the past, due to the bandwidth limitation of most DEP setups, the upper crossover frequency of the real part of the Clausius-Mossotti function was rarely validated. However, with increased bandwidth of current DEP setups, it is important to validate the upper crossover frequency as well as the lower crossover frequency. This will allow DEP to be used to sort or characterize the cytoplasm properties of cells in addition to their membrane properties.

For the first time, we calculated both lower and upper crossover frequencies, f_L and f_U, by using cell parameters R_M, C_M, R_C, and C_C measured on the same UWB setup as that for single-cell DEP. The calculation suggests that in the extreme cases when the uncertainties in R_M, C_M, R_C, C_C, and r_0 all add up, $f_L = 0$–127 kHz and $f_U = 45$–108 MHz. The calculated f_L was found to be in general agreement with the measured f_L, but the calculated f_U was significantly different from the measured f_U. Specifically, the measured $f_L = 28 \pm 4$ kHz, whereas the measured $f_U = 326 \pm 35$ MHz.

The difference between calculated and measured f_U can be attributed to the field being highly nonuniform in single-cell DEP, especially at higher frequencies. This implies that in the future the calculation of f_U needs to be modified by using the field distribution obtained by finite-element simulation. However, simulation in this case is not trivial because it involves bridging the gap between static field on the micrometer scale with wave propagation on the centimeter scale [12]. Additionally, present calculation ignores any adhesive force. With closely spaced electrodes in single-cell DEP, even a relatively nonadherent Jurkat cell, after being trapped, may experience some level of adhesion to the electrodes. Therefore, adhesion force will need to be considered in the calculation in the future. In any case, the difference between the calculated and measured crossover frequency suggests that the classical Clausius-Mossotti function, originally derived from the Maxwell-Wagner mixture model of a cell suspension, may not apply to single-cell DEP in a straightforward manner, especially at high frequencies.

References

[1] H. A. Pohl, *Dielectrophoresis: The Behavior of Neutral Matter in Nonuniform Electric Fields*. New York, NY, USA: Cambridge Univ. Press, 1978.

[2] R. Pethig, *Dielectrophoresis: Theory, Methodology and Biological Applications*. New York, NY, USA: Wiley, 2017.

[3] J. Oblak *et al.*, "Feasibility study for cell electroporation detection and separation by means of dielectrophoresis," *Bioelectrochem.*, vol. 71, no. 2, pp. 164–171, Nov. 2007.

[4] Q. Hu, R. P. Joshi, and A. Beskok, "Model study of electroporation effects on the dielectrophoretic response of spheroidal cells," *J. Appl. Phys.*, vol. 106, no. 2, Jul. 2009, Art. no. 024701.

[5] M. G. Moisescu *et al.*, "Changes of cell electrical parameters induced by electroporation. A dielectrophoresis study," *Biochimica et Biophysica Acta*, vol. 1828, no. 2, pp. 365–372, Feb. 2013.

[6] E. Salimi *et al.*, "Dielectrophoresis study of temporal change in internal conductivity of single CHO cells after electroporation by pulsed electric fields," *Biomicrofluidics*, vol. 11, Feb. 2017, Art. no. 014111.

[7] S. Afshar, E. Salimi, K. Braasch, M. Butler, D. J. Thomson, and G. E. Bridges, "Multi-frequency DEP cytometer employing a microwave sensor for dielectric analysis of single cells," *IEEE Trans. Microw. Theory Techn.*, vol. 64, no. 3, pp. 365–372, Mar. 2016.

[8] S. Afshar *et al.*, "DEP measurement of the dielectric properties of single CHO cells under thermal stress," in *Proc. IEEE MTT-S Int. Microw. Symp. Dig.*, Philadelphia, PA, USA, Jun. 2018, pp. 1152–1155.

[9] F. Hjeij *et al.*, "Biological cell discrimination based on their high frequency dielectropheretic signatures at UHF frequencies," in *Proc. IEEE MTT-S Int. Microw. Symp. Dig.*, Honolulu, HI, USA, Jun. 2017, pp. 533–536.

[10] M. Manczak *et al.*, "Discrimination of glioblastoma cancer stem cells by measuring their UHF-dielectrophoresis crossover frequency," in *Proc. IEEE MTT-S Int. Microw. Biomed. Conf.*, Philadelphia, PA, USA, Jun. 2018, pp. 130–132.

[11] M. Manczak *et al.*, "Tracking cancer cells with microfluidic high frequency DEP cytometer implemented on BiCMOS lab-on-chip platform," in *Proc. IEEE MTT-S Int. Microw. Symp. Dig.*, Philadelphia, PA, USA, Jun. 2018, pp. 104–107.

[12] H. Li *et al.*, "Distributed effect in high-frequency electroporation of biological cells," *IEEE Trans. Microw. Theory Techn.*, vol. 65, no. 9, pp. 3503–3511, Sep. 2017.

[13] X. Du *et al.*, "Validation of Clausius-Mossotti function in single-cell dielectrophoresis," in *Proc. IEEE MTT-S Int. Microw. Biomed. Conf.*, Philadelphia, PA, USA, Jun. 2018, pp. 94–96.

[14] X. Ma, X. Du, H. Li, X. Cheng, and J. C. M. Hwang, "Ultra-wideband impedance spectroscopy of a live biological cell," *IEEE Trans. Microw. Theory Techn.*, vol. 66, no. 8, pp. 3690–3696, Aug. 2018.

[15] J. R. Reitz, F. J. Milford, and R. W. Christy, *Foundations of Electromagnetic Theory*, 4th ed. Boston, MA, USA: Addison-Wesley, 2009.

[16] B. Alberts, *Molecular Biology of the Cell*, 7th ed. New York, NY, USA: Garland, 2017.

[17] A. Irimajiri, T. Hanai, and A. Inouye, "A dielectric theory of 'multi-stratified shell model' with its application to a lymphoma cell," *J. Theor. Biol.*, vol. 78, no. 2, pp. 251–269, May 1979.

[18] Y. Ning *et al.*, "Broadband electrical detection of individual biological cells," *IEEE Trans. Microw. Theory Techn.*, vol. 62, no. 9, pp. 1905–1911, Sep. 2014.

[19] X. Ma *et al.*, "Sensitivity analysis for ultra-wideband 2-port impedance spectroscopy of a live cell," *IEEE J. Electromagn. RF Microw. Med. Bio.* to be published.

[20] X. Du *et al.*, "Ultra-wideband characterization, electroporation, and dielectrophoresis of a live biological cell using the same vector network analyzer," in *Proc. IEEE MTT-S Int. Microw.*, Philadelphia, PA, USA, Jun. 2018, pp. 1148–1151.

[21] H. Li *et al.*, "Correlation between optical fluorescence and microwave transmission during single-cell electroporation," *IEEE Trans. Biomed. Eng.*, doi/10.1109/TBME.2018.2885781.

Xiaotian Du (S'17) received the B.S. degree in materials science from Fudan University, Shanghai, China, in 2016. He is currently working toward the Ph.D. degree in electrical engineering with Lehigh University, Bethlehem, PA, USA, since the fall of 2016. In 2014, he was exchange student with the University of California at Berkeley. Since July 2015, he has been working as a Research Assistant in electrical engineering with Lehigh University. His research interest includes biosensors, MEMS, and other microwave devices and circuits.

Xiao Ma (S'15) received the B.S. degree in physics from Peking University, Beijing, China, in 2014. He is currently working toward the Ph.D. degree with Lehigh University, Bethlehem, PA, USA. In the summer of 2013, he was a Research Assistant with Georgia Tech Lorraine on BIMDM structures. His current research interest includes biosensor, microwave measurement, and liquid calibration. He specializes in 3-D electromagnetic simulation using finite element methods and microwave device characterization techniques.

Hang Li (M'16) received the B.S degree in chemical engineering and technology from Xi'an Shiyou University, Xi'an, China, in 2009 and the Ph.D. degree in chemical and biomolecular engineering from The University of Akron, OH, USA, in 2015. Since 2015, he has been a Research Associate with Lehigh University, Bethlehem, PA, USA. His research interest includes mammalian cell electroporation and cell/bacterial membrane dynamic detection by broadband sensing.

Lei Li (S'17) received the B.S degree in electrical engineering from the University of Science and Technology of China, Hefei, China, in 2016. He is currently working toward the Ph.D. degree in electrical engineering with Lehigh University, Bethlehem, PA, USA. His research interest includes novel devices, circuits, and their applications.

Xuanhong Cheng received the B.S. degree in biology from Wuhan University, Wuhan, China, in 1998 and the M.S. degree in electrical engineering and the Ph.D. degree in bioengineering from the University of Washington, Seattle, WA, USA, in 2004. After Postdoctoral training with the Department of Surgery at Massachusetts General Hospital, she joined Lehigh University, Bethlehem, PA, USA, in 2008, where she is currently an Associate Professor with the Bioengineering Program and Department of Materials Science and Engineering. The focus of her research is to develop microfluidic devices for cell and pathogen analysis. In combination with nanomaterials and biosensors, these devices are expected to perform automated sample processing and sensitive analytic detection toward point-of-care uses.

James C. M. Hwang (M'81–SM'82–F'94–LF'15) received the B.S. degree in physics from National Taiwan University, Taipei, Taiwan, and the M.S. and Ph.D. degrees in materials science and engineering from Cornell University, Ithaca, NY, USA. Since 1988, he has been a Professor of electrical engineering and the Director of Compound Semiconductor Technology Laboratory, Lehigh University, Bethlehem, PA, USA. Prior to that, he spent 12 years with IBM, Bell Labs, GE, and GAIN. He cofounded GAIN and QED; the latter became a public company (IQE). He has worked on microwave materials, devices, and circuits for four decades.